Volume 10
Number 4
28 January 2018
Pages 1549-2172

Nanoscale

rsc.li/nanoscale

ISSN 2040-3372

PAPER
Shuping Xu, Chongyang Liang *et al.*
Organelle-targeting surface-enhanced Raman scattering
(SERS) nanosensors for subcellular pH sensing

ROYAL SOCIETY OF CHEMISTRY

NCNST

ROYAL SOCIETY OF CHEMISTRY

rsc.li/nanoscale

Unveiling the origin of room-temperature ferromagnetism in monolayer VSe₂: the role of extrinsic effects

Danil W. Boukhvalov[1,2,*], and Antonio Politano[3,4]

[1]*College of Science, Institute of Materials Physics and Chemistry, Nanjing Forestry University, Nanjing 210037, P. R. China*

[2]*Institute of Physics and Technology, Ural Federal University, Mira Street 19, 620002 Yekaterinburg, Russia*

[3]*Department of Physical and Chemical Sciences, University of L'Aquila, via Vetoio, 67100 L'Aquila (AQ), Italy*

[4]*CNR-IMM Istituto per la Microelettronica e Microsistemi, VIII strada 5, I-95121 Catania, Italy*

ABSTRACT

Room-temperature ferromagnetism in monolayer vanadium diselenide (VSe₂) on graphite is object of a controversial debate. Herein, we unveil the contribution from extrinsic factors to the magnetic properties of monolayer VSe₂ by means of density functional theory. Specifically, we demonstrate that either intrinsic defects or adsorption of molecules enhance ferromagnetic interactions. The expansion of the VSe₂ lattice increases the magnetic moment on vanadium ions, whereas both compression and out-of-plane distortion withdraw magnetic moments. The exchange interactions between vanadium ions and magnetic defects (vacancies and iron impurities) in surface and subsurface layers of the substrate are able to turn the unstable two-dimensional (2D) ferromagnetism into stable three-dimensional (3D) ferromagnetism. The combination of effects related to chemisorption, substrate-induced distortion and magnetic defects of the substrate could enhance or suppress ferromagnetism in monolayer VSe₂.

Corresponding Author*: * danil@njfu.edu.cn*

1. Introduction

Monolayer VSe₂, in the family of 2D transition-metal dichalcogenides, is triggering the interest of the scientific community due to several recent discoveries, including in-plane piezoelectricity,[1] a pseudogap with Fermi arc[2] at temperatures above the charge-density-wave

(CDW) transition temperature (~220 K in the monolayer),[3] and especially the emergence of room-temperature ferromagnetism.[4-11] However, experimental findings related to ferromagnetism remain controversial. Specifically, recently, room-temperature ferromagnetism with a giant magnetic moment of ~15 μ_B per formula unit has been reported for monolayer VSe_2 epitaxially grown on graphite.[4] Local magnetic phase contrast has also been observed by magnetic force microscopy at room temperature at the edges of VSe_2 flakes exfoliated from a three-dimensional crystal.[12] However, both Feng *et al.*[13] and Chen *et al.*[3] reported the absence of exchange splitting at the V $3d$ bands by angle-resolved photoemission spectroscopy for monolayer VSe_2 grown on bilayer graphene/SiC substrate, in contrast with another study obtaining a magnetization value not higher than ~5 μ_B.[14] Other researches even reported the emergence of anti-ferromagnetism in selenium defects-abundant areas of VSe_2 monolayer.[15,16]

Many theoretical models have been recently developed in order to account for the above-mentioned discrepant observations.[4,12,14] For instance, it has been suggested that the presence of CDW could cause the quenching of monolayer ferromagnetism, due to the band-gap opening induced by Peierls distortion in bulk Vse_2.[17] Note that in another recent work, imaginary modes in phonon spectra of non-magnetic VSe_2 were reported, which disappear in the spectra calculated for ferromagnetic configuration,[18] similarly to previous reports for ReS_2.[19] The possible origin of this unexpectedly strong relationship between magnetic and structural properties was ascribed[18] to be the overlap between $3d$ bands of V and $4p$ bands of Se. Both theory[18] and experiment[20] demonstrate possibility of the transition between *2H* and *1T* configurations at ambient conditions. Another relevant issue is related to the structural properties of monolayer VSe_2, considering the contradiction between theoretically reported *2H* configuration as ground state[16,21] and the experimental evidence of a band-structure typical of *1T* configuration.[13,14,15] Recent experimental[22] and theoretical[23] reports about influence of magnetic substrate on magnetic properties of VSe_2 suggest that possible magnetic defects in the substrate could influence magnetic properties of VSe_2 on graphitic substrate.

Indeed, the magnetic properties of monolayer VSe_2 could be affected by any defects (vacancies, impurities) or extrinsic intervention, such as the adsorption of environmental contaminants or substrate-induced distortion. In this work, we consider the effects on magnetisms related to (i) the adsorption of molecular oxygen and water in vicinity of Se-vacancy sites, (ii) the presence of carbon impurities and (iii) the effect of in-plane (expansion

and compression of atomic lattice) and out-of-plane distortions. We clarify that the violation of two dimensionality is essential for existence of room temperature magnetism in systems such as VSe_2. Moreover, we elucidated the effects of the underlying substrate by modelling the magnetic interactions between V atoms and intrinsic (dangling bonds) and extrinsic (iron impurities) magnetic defects in the graphitic substrate.

2. Computational Method

Theoretical modeling was performed by DFT using the Quantum ESPRESSO code[24] and the GGA–PBE + van der Waals (vdW) approximation,[25,26] feasible for the description of the adsorption of molecules on surfaces of dichalcogenides. We used energy cutoffs of 25 and 400 Ry for the plane-wave expansion of the wave functions and the charge density, respectively, and the 4×4×3 Monkhorst-Pack k-point grid for the Brillouin sampling.[29]

To investigate the role of adsorption and decomposition of molecules on magnetic properties of VSe_2, we considered adsorption of molecular oxygen and water (the most abundant oxidative species in the air) on 3×3 supercell. We considered both *1T* and *2H* configurations of VSe_2 (see Fig. 1). As we discuss adsorption on monolayer, optimization of atomic positions and lattice parameters were performed. We estimate the energetics corresponding to these processes in terms of differential enthalpy ΔH:

$$\Delta H = E_{final} - E_{initial},$$

where $E_{initial}$ and E_{final} denote the total energies for molecules far from the VSe_2 surface (set at a distance of about 8 Å) and for adsorbed molecules (Figure 1a), respectively.

To evaluate the decomposition, the initial configuration is associated with molecular adsorption on VSe_2, while the final configuration implies the formation of covalent bonds with the fragments of the decomposed molecule (Figure 1b). In addition to pristine VSe_2 with no defects, we also considered (i) Se vacancies (Figure 1a), which are expected to exist at the grain boundaries and edges of monolayer VSe_2, and (ii) Se substitution by C atoms from the substrate. The latter concerns hypothetic possible incorporation of surface C atoms from the graphite substrate. Here, we consider a concentration of selenium vacancies of 5.5%.

For modeling biaxial strain, we changed lattice parameter by 1% at each step, with further optimization of atomic positions at fixed lattice parameters.

3. Results and discussions

3.1. Effect of defects and adsorption on magnetism
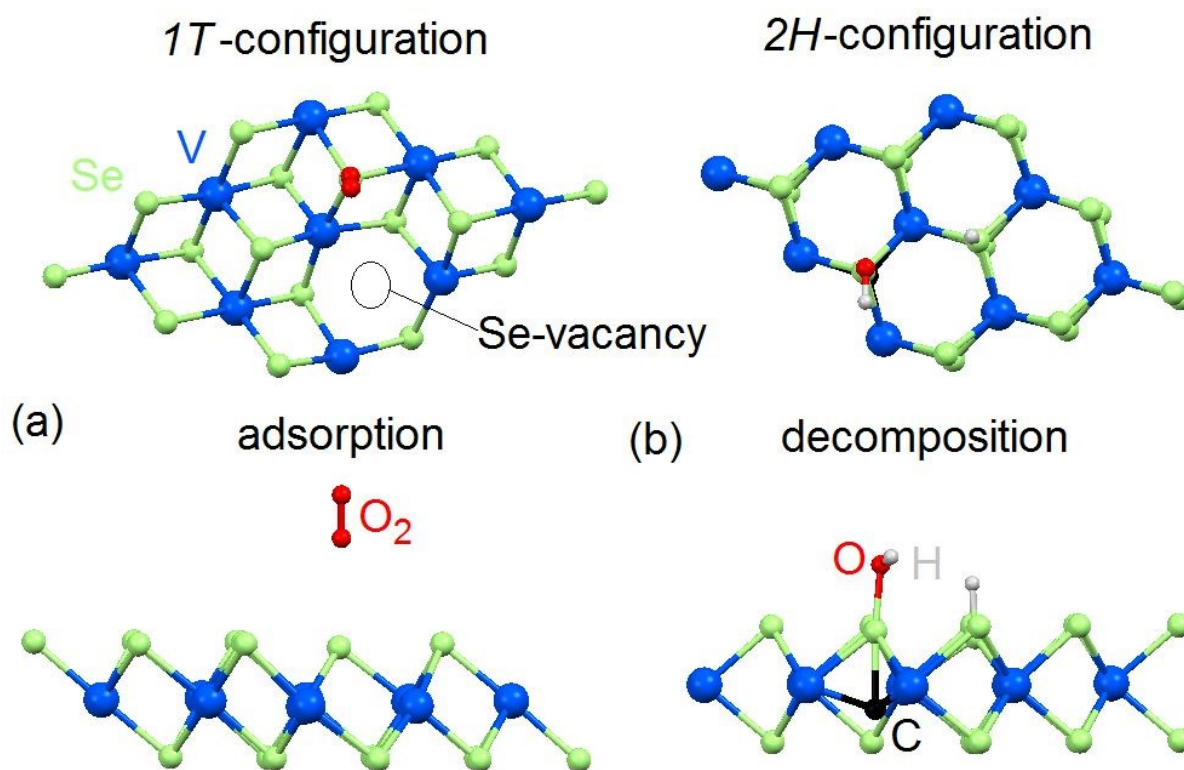
Figure 1. Optimized atomic structure of (a) molecular oxygen adsorbed on T-VSe$_2$ with a Se vacancy and (b) decomposed water molecule on H-VSe$_2$ with a carbon impurity. Green, blue, white, red and black balls denote Se, V, H, O and C atoms, respectively.

To determine how defects and chemisorbed species influence the magnetic properties of the monolayer, we calculated the magnetic moment and exchange integral. The latter parameter is evaluated from the energy difference between the ferromagnetic (E_{FM}) and antiferromagnetic (E_{AFM}) ordering, based on Heisenberg's approximation:

$$E_{FM} - E_{AFM} = -NS^2J,$$

where J is the exchange integral, S is the spin (½, given the d^1 electronic configuration of VSe₂) and N is the number of exchange interactions influenced by rotation of the spin, which is 6 for the present case. To imitate antiferromagnetic configuration, we changed orientation of the spin on single V ion in the supercell and perform calculation of total energy without further optimization of atomic structure. According to our self-consistent calculations, ferromagnetic exchange interactions are for most cases notable (positive J in Table I), resulting in parallel oriented spins from initially antiparallel oriented ones. For multiple cases, in spite of the initial antiferromagnetic configuration, self-consistent calculations indicated the emergence of a ferromagnetic configuration (robust ferromagnetism in Table 1, with estimated J>10,000 K.
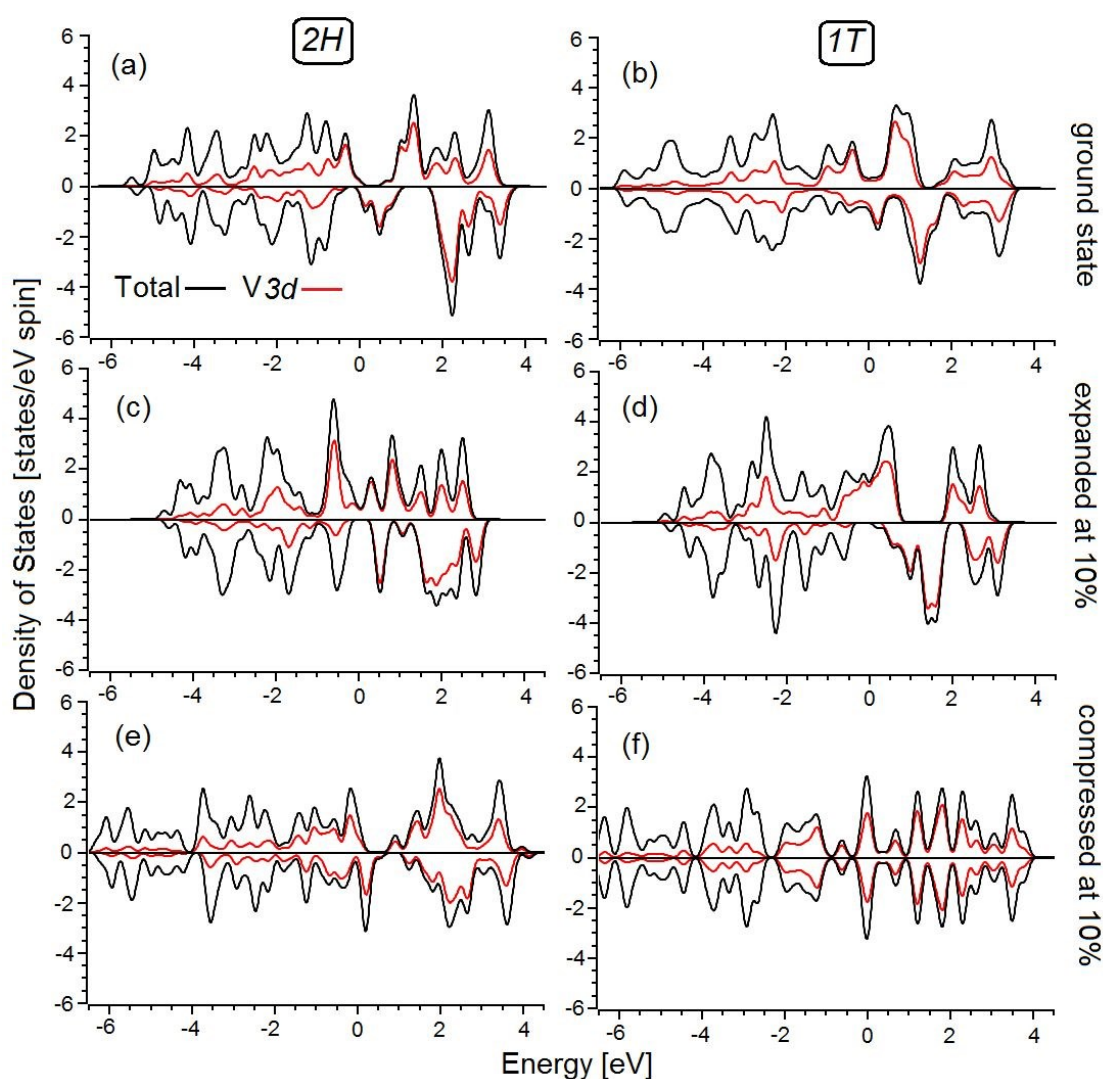
Figure 2. Total densities of states (black lines) and partial densities of states of *3d* orbitals of V atomic (red lines) for ground state (a, b), uniaxial expanded (c, d) and compressed (e, f) *2H* (a, c, e) and *1T* configurations of VSe₂. All data are reported for ferromagnetic configurations. Fermi energy is set as zero.

Note that the Heisenberg model is exact only in systems, such as V_{15} clusters, where $3d$ bands are well-separated from the $2p$, $3p$ or $4p$ bands.[30] Considering the significant overlap between the V $3d$ and Se $4p$ bands of VSe_2 in both structural configurations (Figs. 2a,b), our model can thus reliably estimate the influence of structural configuration, defects and chemisorption on the magnetic properties of the monolayer.

Table I shows that the *H*- and *T*-phase VSe_2 exhibit different values of V magnetic moments and magnitudes of exchange interactions, due to their different electronic structures (Figs. 1a,b). Moreover, the differential enthalpy for physisorption of both oxygen and water on the pristine, perfect surface is positive, indicating that their adsorption is energetically unfavorable in all cases. Consequently, stable adsorption of O, H, and OH species from decomposition of oxygen and water becomes impossible, and thus pristine VSe_2 without defects can be regarded as chemically inert. Our conclusions are validated by vibrational experiments on monolayer VSe_2 reported in Electronic Supplementary Information, Figure S1.

Table I. Calculated values of magnetic moments m (in μ_B), exchange integrals J (in K) and differential enthalpy of O_2 and H_2O adsorption and decomposition (in meV) on VSe_2. Both the *H* and *T* phases of VSe_2 have been considered, with the monolayer either in pristine form or with defects, such as Se vacancies (v_{Se}) and C substitutions (C_{Se}). Stable adsorption is reported in bold. For the cases of physisorption and chemisorption, we report magnetic moments of V atoms in the first and third coordination sphere from the adsorption site. The abbreviation RFM corresponds to the instability of antiferromagnetic configuration.

Substrate		Before adsorption		After O_2 physisorption [H_2O]			After O_2 decomposition [H_2O]		
quality	type	m (μ_B)	J (K)	ΔH (meV)	m (μ_B)	J (K)	ΔH (meV)	m (μ_B)	J (K)
undefected	*2H*	0.93	RFM	1,069 [14]	0.91 [0.92]	RFM [RFM]	-1,430 [1,576]	0.84, 0.93 [0.64, 0,76]	RFM [RFM]
	1T	0.69	+192	48 [113]	0.64 [0.65,0.57]	+3,103 [RFM]	-40 [1,376]	0.30, 0.85 [0.08, 0.51]	+159 [RFM]
v_{Se}	*2H*	1.09, 0.74	3,400	**-54** [34]	1.07, 0.72 [1.04, 0.74]	RFM RFM	**-4,086** [1,780]	0.67, 0.74 [1.11, 0.37]	RFM [815]
	1T	1.09, 0.54	+1,068	683	0.923, 0.66	RFM	-662	0.01, 0.27	RFM

				[-89]	[1.06, 0.74]	[RFM]	[561]	[0.08, 0.34]	[RFM]
C_{Se}	2H	0.64, 0.73	+1,706	5 [-193]	0.34, 0.57 / 0.65, 0.74	-13 [RFM]	-155 [+1,867]	0.21, 0.55 / 0.12, 0.53	RFM [RFM]
	1T	0.31, 0.65	RFM	-11 [-160]	0.29, 0.63 [0.32, 0.59]	RFM [RFM]	+62 [+2.415]	0.24, 0.44 [0.11, 0.61]	RFM [RFM]

From Table I, we can also find that the presence of defects induces local modifications of magnetic moments. Specifically, in the presence of Se vacancies, the adsorption of O_2 is energetically favorable on 2H-VSe_2 (due to the negative ΔH), while it is unfavorable on the 1T-phase counterpart. In contrast, H_2O adsorption is energetically favorable on 1T-VSe_2 but not on 2H-VSe_2. Combined with the calculated ΔH for the decomposition, we conclude that further decomposition of molecular adsorbates is only possible for O atoms in the vicinity of Se vacancies in 2H-VSe_2, where ΔH for adsorption and decomposition are both negative. Accordingly, we can assert that defect sites of VSe_2 create exclusive adsorption sites for ambient gases. Furthermore, the possible substitution of Se atoms by C atoms from the substrate also enables molecular adsorption of H_2O on both VSe_2 phases, whereas O_2 adsorption is only feasible for 1T-VSe_2. Our findings indicate that the presence of substitutional C atoms effectively increases the energy cost for surface decomposition, compared with pristine and Se-deficient VSe_2.

As also shown in Table I, physisorption of chemical species leads to a significant increase in the magnitude of the exchange integral, while it does not considerably alter the values of V magnetic moments. The former originates from molecular doping from adsorbates, which favors exchange via electrons from bands crossing the Fermi level. Local distortions of the atomic structure (Figure 1a) induced by physisorption can also affect exchange interactions, which are highly sensitive to symmetry violation.[31,32] Nevertheless, one remarkable exception exists for O_2 adsorption on C-substituted 2H-VSe_2, for which the combination of (i) the substitution of Se^{2+} by a C atom with (ii) further adsorption and decomposition of O_2 decreases the magnetic moment and turns its J from positive to negative (i.e. from ferro- to antiferromagnetic). However, given a positive differential enthalpy, such a physisorption is unlikely to occur.

Further decomposition of the adsorbed molecules decreases the magnetic moments on V ions, and results in the formation of covalent Se-O bonds which change the oxidation state of V from 4+ to 5+, associated with a $d^1 \rightarrow d^0$ transition. Despite these variations in both atomic and electronic structures, the exchange interactions remain robust; neither physical nor chemical adsorption of gases can destroy the strong ferromagnetism of monolayer VSe_2. The key conclusion from our calculations is that oxide formation of air-exposed VSe_2 is energetically favorable only for $2H$-VSe_2 with physically adsorbed H_2O in the vicinity of Se vacancies, but the missing experimental observation of $2H$ configuration of VSe_2 makes this scenario a rather limited case in real conditions. Based on results of the calculations, we can assert that neither defects nor adsorption could originate the suppression and vanishing of ferromagnetism in both structural configurations of monolayer VSe_2. Conversely, the presence of defects and adsorption usually leads to enhancement of ferromagnetic interactions.
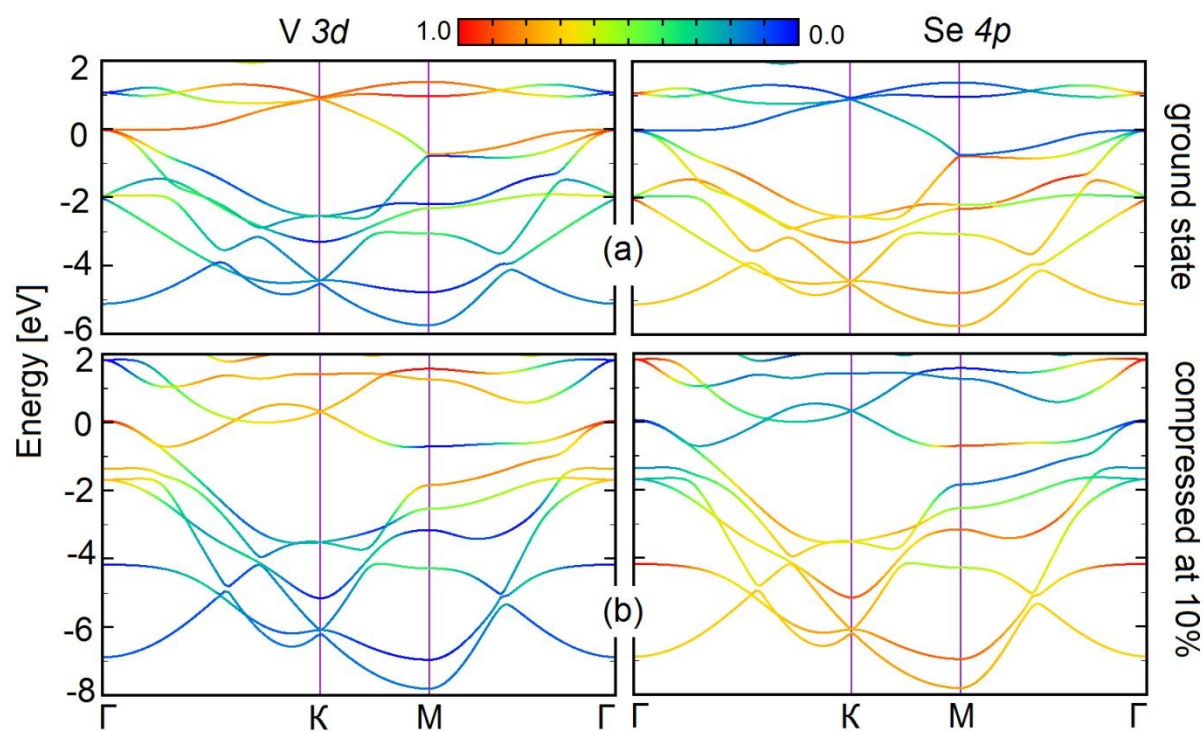

Figure 3. Orbital-projected band structure of V-$3d$ and Se-$4p$ orbitals for $1T$-VSe_2 in (a) its ground state and (b) after biaxial compression of 10% (b). The Fermi energy is set as zero.

3.2. Influence of lattice distortion on magnetic properties

We explored the effects of lattice distortions on magnetic properties of monolayer VSe_2, considering that (i) the significant entanglement between V $3d$ and Se $4p$ bands (see Fig. 3a)

makes VSe_2 different from other V^{4+}-compounds with distinct d^1 peak near Fermi level[30] and (ii) phonon spectra of non-magnetic and magnetic configurations are very different.[18] The simplest kind of lattice distortions is the in-plane extension or compression of membrane. Considering that monolayer VSe_2 is supported by substrates with hexagonal symmetry, such as graphite[4] and MoS_2[16], the mismatch of the lattice parameters can induce only biaxial strain. Our theoretical model (Fig. 4a) indicates that the energy cost for the expansion of the atomic lattice is smaller than the energy cost for compression. The value of the thermal energy per mole at room temperature is about 25 meV, corresponding to a modification of the lattice parameter smaller than on 3%, with negligible effects on magnetic properties. Similar effects were discussed for the tiny displacement of the single Se atom from its stoichiometric position.[18] Thus, we can rule out an eventual influence of temperature-induced in-plane-distortion on the magnetic properties of VSe_2.
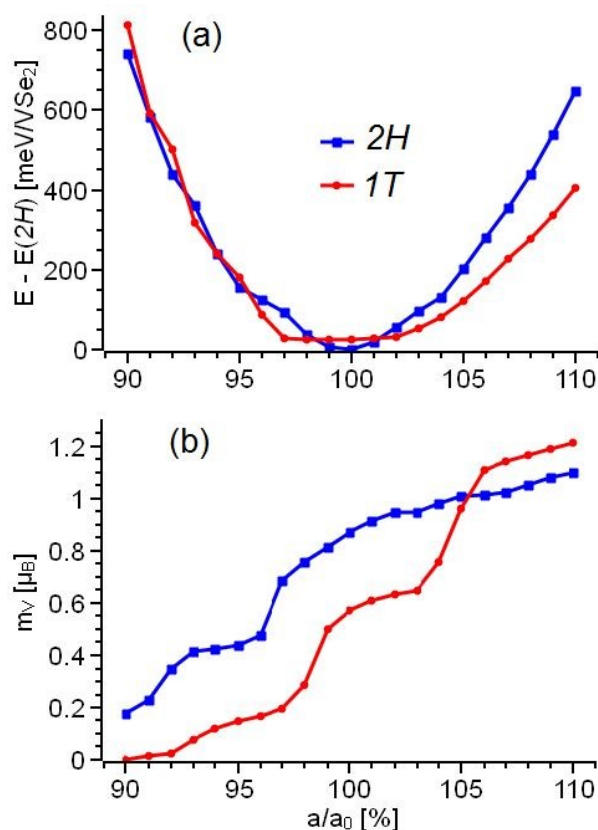

Figure 4. (a) Difference of the total energy of uniaxial compressed or expanded monolayer VSe_2 and total energy in ground state (undistorted *2H* configuration) and (b) magnetic moment on V atoms as function of the change of lattice parameter *a* from 90% to 110% of the ground state value (a_0).

Upon expansion above 3%, the *1T* configuration results to be more energetically favorable. Moreover, a weak compression (in the range 2-4%) also makes the *1T* configuration more stable than the *2H*. These results explain why, in spite of lower total energy of *2H* configuration, angle-resolved photoemission spectroscopy (ARPES) measurements detected band-structure corresponding with *1T* configuration.[13,14,15] Substrate-induced distortion of the lattice makes *1T* configuration more energetically favorable. Varying the lattice parameter also provides changes of V-Se-V angles, which influence the electronic structure of the whole system in both considered structural configurations. Expanding the lattice provides narrowing of valence and conductive bands (Fig. 2c,d) and compression of the lattice, leading to widening of these bands (Fig. 2e,f).

Such changes in the electronic structure are related to the modification of Se-V-Se angles, with subsequent changes in the crystal field. Moreover, energy shifts of related orbitals (Fig. 3) are originated by the entanglement between V-*3d* and Se-*4p* bands (Fig. 3b), arising from the formation of hybrid V-Se orbitals. Specifically, the d^1 electron, originally localized on V-*3d* shell, becomes spread over such delocalized V-Se orbitals.

These modifications in electronic structure provide changes of magnetic moments of V ions. Expansion of the lattice corresponds with increasing values of magnetic moments, while compression leads to a decrease of magnetic moments (see Fig. 4b). Compression of *1T*-VSe_2 at 8% leads to decreasing of the values of magnetic moments below 0.05 μ_B with further vanishing of the magnetism in system.
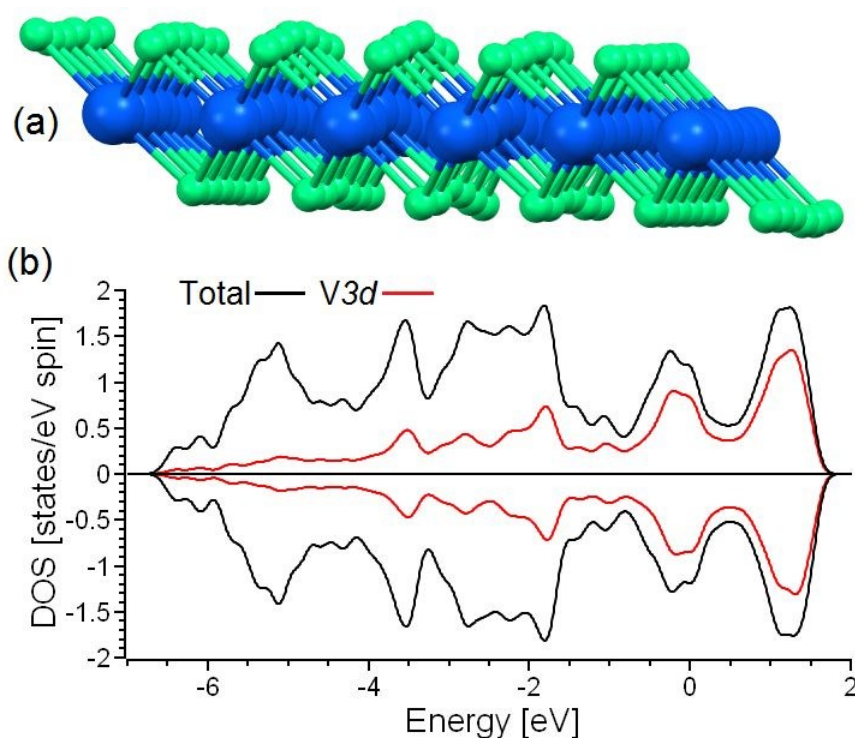
Figure 5. Optimized atomic structure of (a) ripple created on VSe$_2$ supercell and (b) its electronic structure.

Our results indicate a colossal effect of the lattice distortion on magnetic properties of VSe$_2$. Huge compression of the lattice inducing the disappearance of magnetic moments on V atoms is rather improbable but provides a clue for the further modelling. Actually, some substrates on which VSe$_2$ was supported are able create not only in-plane strain but also out-of-plane distortions. We will consider only one kind of out-of-plane distortion, i.e., ripples. This type of the distortion corresponds with the formation of hill-like puckering of the membrane (see Fig. 4a). For modelling the ripple, we build 6×6 supercell of 108 atoms, with decreased lattice parameter by 5%. Initially, we shift-up some atoms in the center and optimized atomic positions for fixed lattice parameters. This initial shift-up of some atoms guides formation of the ripple in the center of the supercell. In contrast to the calculations of compressed lattice, in this case out-of-plane motion of atoms leads to the restoration of the values of V-V distances to the same as in ground state, although V-Se-V angles slightly changed (2.1~2.4°) on the top of the ripple. The restoration of V-V distances provides decreasing of the energy cost of the formation from 209 meV/VSe$_2$ for in-plane compression to 154 meV/VSe$_2$ in the case of ripple. Taking into account that at room temperature the value of thermal energy per mole is about 25 meV, we can consider this distortion of flat monolayer

VSe$_2$ to be substrate-induced rather than intrinsic. The formation of this ripple of modest height (0.33 Å) leads to a decreasing magnetic moments on V atoms down to the values 0.02~0.07μ$_B$, which is three times smaller with respect to the case of in-plane compression of the lattice at 5% (Fig. 5b). To reveal the possible effect of the compression on the vanishing of magnetic moments, we compared the electronic structure of supercell with ripple (Fig. 5b) with that related to the only in-plane compression. Formation of the ripple does not provide broadening of valence and conduction bands observed for compressed flat VSe$_2$ monolayer (Fig. 2e,f). Thus, vanishing of magnetic moments on V atoms cannot be attributed to in-plane compression of the lattice and out-of-plane distortion of the lattice, as well as to changes of V-Se-V angles that change crystal field and shift Se *4p* bands towards of Fermi level. In the case of undistorted *1T*-VSe$_2$, the total density of states below Fermi level almost coincides with the total density of states (Fig. 2b) in contrast to buckled VSe$_2$ (Fig. 5b). These changes in the energetics of bands increase the entanglement of V-*3d* and Se-*4p* bands, leading to the formation of hybrid V-Se bands and to the delocalization of d^1 electron on V-*3d* shell. Note that this huge effect on electronic structure and magnetic properties is caused by rather modest out-of-plane distortions, which can be even originated by any substrate.

3.3. Interactions with magnetic centers in substrate

In previous paragraphs, we discussed only in-plane magnetic interactions. Previously, spin fluctuations were shown to destabilize 2D ferromagnetism in some metals and semiconductors at room temperature.[33,34] On the other hand, all reports about ferromagnetism in VSe$_2$ were provided for its monolayer on graphite. It is important to point out that interaction of V ions and magnetic centers in graphite substrate will transform magnetic system from 2D into 3D. Definitely, two types of magnetic centers are known to exist in graphite: (i) magnetic defects, such as grain boundaries or point defects,[35,36] and (ii) magnetic impurities, i.e. contamination by magnetic ions of transitional metals.[37]
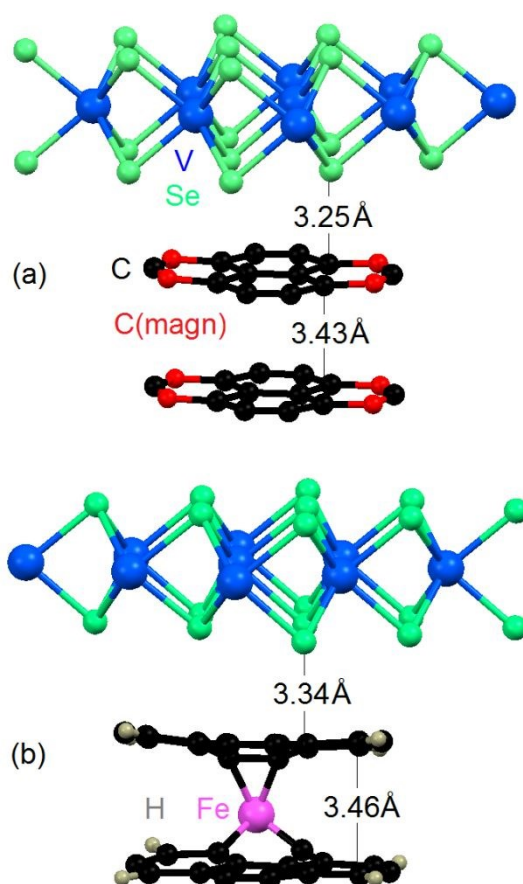
Figure 6. Optimized atomic structure and interlayer distances of VSe_2 on (a) bilayer graphite with magnetic moments on dangling bonds on the edges and (b) over bilayer graphite with passivated edges and one Fe atom in-between layers. C atoms with dangling bonds are shown in red.

To illustrate the interaction with the point defects in graphite, we modeled a monolayer VSe_2 on top of two surface layers of graphite (Figure 6a). We find that dangling bonds at the non-passivated graphite edges represent a source of magnetic moments with a magnitude of ~0.17 μ_B. After optimization of atomic positions, we computed the energy difference between two magnetic configurations with parallel and antiparallel orientation of magnetic moments on VSe_2 monolayer and magnetic graphite substrate. We find that, for both phases of VSe_2, the parallel orientation is more energetically favorable than the antiferromagnetic one. Quantitatively, the values of exchange interactions are 531 and 460 K per each V-C (magnetic) exchange for the *2H* and *1T* phases of VSe_2, respectively. The large magnitude of the exchange interactions corresponds to a charge transfer from VSe_2 to substrate of about 0.27 and 0.23 electrons per VSe_2 in the *2H* and *1T* phases, respectively, which are sufficiently large to activate ferromagnetism at room temperature. We note that a similar mechanism was proposed in Ref. [4] for the case of monolayer VSe_2 on MoS_2, congruently with our theoretical findings. Figure 6b depicts another model to establish the interaction with

the magnetic impurities in graphite. The most abundant of such impurities are known to mainly derive from Fe ions, in spite of their existence being often below the detection limit of conventional techniques, such as X-ray photoelectron spectroscopy.[37] The model consists of a VSe_2 monolayer on top of two layers of graphite with passivated edges and an intercalated Fe atom in between their interlayer gap. In this case, the resulting 3D ferromagnetism is very robust and exhibits values of the exchange interactions up to 2986 and 870 K per each Fe-V exchange for the *2H* and *1T* phases, corresponding to a VSe_2-substrate charge transfer of 0.28 and 0.21 electrons per VSe_2, respectively. Definitely, calculations evidence existence of robust ferromagnetic interactions between VSe_2 monolayer and magnetic centers in substrate located up to a distance of 3~7 Å. The abundance of these centers leads to the appearance of ferromagnetism at room temperature, with the subsequent detection of surprisingly large magnetic moments per V ions.[14] Contrary, in the case of missing magnetic defects in the substrate, ferromagnetism in VSe_2 remains two-dimensional and unstable

4. Conclusions

Our first-principles calculations demonstrate that neither defects nor physisorption/chemisorption of water and oxygen are able to quench ferromagnetism in monolayer VSe_2. Additionally, adsorption of oxygen and water on VSe_2 monolayer is rather unlikely. On the other hand, in the cases of in-plane compression of out-of-plane distortions, magnetic moments vanish on vanadium centers. Our modelling also demonstrates the possibility of the robust ferromagnetic interactions between monolayer VSe_2 and magnetic defects in graphitic substrate. These ferromagnetic interactions provide stabilization of thermally unstable 2D ferromagnetism by transformation of magnetic system to 3D. Thus, we can propose that the joint effect of substrate-induced distortions of monolayer VSe_2 and the presence of magnetic defects in graphitic substrate should be considered as responsible of the controversial results in literature concerning magnetic properties of monolayer VSe_2, ranging from missing magnetism up to strong ferromagnetism at room temperature.

Acknowledgements

Nanoscale Accepted Manuscript

References

[1] J. Yang, A. Wang, S. Zhang, J. Liu, Z. Zhong, L. Chen, Phys. Chem. Chem. Phys. 2019, **21**, 132.

[2] Y. Umemoto, K. Sugawara, Y. Nakata, T. Takahashi, T. Sato, Nano Res. 2019, **12**, 165.

[3] P. Chen, W.W. Pai, Y. H. Chan, V. Madhavan, M.Y. Chou, S.K. Mo, A.V. Fedorov, T. C. Chiang, Phys. Rev. Lett. 2018, **121**, 196402.

[4] M. Bonilla, S. Kolekar, Y. Ma, H. C. Diaz, V. Kalappattil, R. Das, T. Eggers, H. R. Gutierrez, M.-H. Phan, M. Batzill, Nature Nanotechnology 2018, **13**, 289.

[5] Q. Wu, Y. Zhang, Q. Zhou, J. Wang, X. C. Zeng, J. Phys. Chem. Lett. 2018, **9**, 4260.

[6] Z. Wang, T. Zhang, M. Ding, B. Dong, Y. Li, M. Chen, X. Li, J. Huang, H. Wang, X. Zhao, Y. Li, D. Li, C. Jia, L. Sun, H. Guo, Y. Ye, D. Sun, Y. Chen, T. Yang, J. Zhang, S. Ono, Z. Han, Z. Zhang, Nat. Nanotechnol. 2018, **13**, 554.

[7] D. J. O'Hara, T. Zhu, A. H. Trout, A. S. Ahmed, Y. K. Luo, C. H. Lee, M.R. Brenner, S. Rajan, J. A. Gupta, D. W. McComb, R. K. Kawakami, Nano Lett. 2018, **18**, 3125.

[8] S. Jiang, L. Li, Z. Wang, K. F. Mak, J. Shan, Nat. Nanotechnol. 2018, **13**, 549.

[9] N.C. Frey, H. Kumar, B. Anasori, Y. Gogotsi, V. B. Shenoy, ACS Nano 2018, **12**, 6319.

[10] D.V. Averyanov, I.S. Sokolov, A.M. Tokmachev, O.E. Parfenov, I.A. Karateev, A.N. Taldenkov, V.G. Storchak, ACS Appl. Mater. Interfaces 2018, 10, 20767.

[11] N. Samarth, Nature 2017, **546**, 216.

[12] S. Lee, J. Kim, Y. C. Park, S.-H. Chun, Nanoscale 2019, **11**, 431.

[13] J. Feng, D. Biswas, A. Rajan, M. D. Watson, F. Mazzola, O. J. Clark, K. Underwood, I. Marković, M. McLaren, A. Hunter, D. M. Burn, L. B. Duffy, S. Barua, G. Balakrishnan, F. Bertran, P. Le Fèvre, T. K. Kim, G. van der Laan, T. Hesjedal, P. Wahl, P. D. C. King, Nano Lett. 2018, **18**, 4493.

[14] G. Duvjir, B. K. Choi, I. Jang, S. Ulstrup, S. Kang, T. Thi Ly, S. Kim, Y.H. Choi, C. Jozwiak, A. Bostwick, E. Rotenberg, J.-G. Park, R. Sankar, K.-S. Kim, J. Kim, Y.J. Chang, Nano Lett. 2018, **18**, 5432.

[15] P.K.J. Wong, W. Zhang, F. Bussolotti, X. Yin, T.S. Herng, L. Zhang, Y.L. Huang, G. Vinai, S. Krishnamurthi, D.W. Bukhvalov, Y.J. Zheng, R. Chua, A.T. N'Diaye, S.A. Morton, C.-Y. Yang, K.-H.O. Yang, P. Torelli, W. Chen, K.E.J. Goh, J. Ding, M.-T. Lin, G. Brocks, M. P. de Jong, A. H. Castro Neto, A.T.S. Wee, Adv. Mater. 2019, **31**, 1901185.

[16] R. Chua, J. Yang, X. He, X. Yu, W. Yu, F. Bussolotti, P. Kwan, J. Wong, K.P. Loh, M.B.H. Breese, K.E. Johnson Goh, Y.L. Huang, A.T.S. Wee, Adv. Mater. 2020, **32**, 2000693.

[17] A.O. Fumega, M. Gobbi, P. Dreher, W. Wan, C. González-Orellana, M. Peña-Díaz, C. Rogero, J. Herrero-Martín, P. Gargiani, M. Ilyn, M. M. Ugeda, V. Pardo, S. Blanco-Canosa, J. Phys. Chem. C 2019, **123**, 27802.

[18] G.V. Pushkarev, V.G. Mazurenko, V.V. Mazurenko, D.W. Boukhvalov, Phys. Chem. Chem. Phys. 2019, 21, 22647.

[19] S. Divilov, W. Wan, P. Dreher, M.M. Ugeda, F. Yndurain, arXiv:2005.06210 2020.

[20] G. Duvjir, B.K. Choi, T.T.Ly, N.H. Lam, S.-H. Chun, K. Jang, A. Soon, Y. J. Chang J. Kim, Nanoscale 2019, **11**, 20096.

[21] Y. Ma, Y. Dai, M. Guo, C. Niu, Y. Zhu and B. Huang, ACS Nano, 2012, **6**, 1695.

[22] G. Vinai, C. Bigi, A. Rajan, M. D. Watson, T.-L. Lee, F. Mazzola, S. Modesti, S. Barua, M. Ciomaga Hatnean, G. Balakrishnan, P. D. C. King, P. Torelli, G. Rossi, and G. Panaccione Phys. Rev. B 2020, **101**, 035404.

[23] F. Zhang, W. Mi, X. Wang, Nanoscale 2019, **11**, 10329.

[24] P. Giannozzi, S. Baroni, N. Bonini, M. Calandra, R. Car, C. Cavazzoni, D. Ceresoli, G. L. Chiarotti, M. Cococcioni, I. Dabo, A. Dal Corso, S. de Gironcoli, S. Fabris, G. Fratesi, R. Gebauer, U. Gerstmann, C. Gougoussis, A. Kokalj, L. Michele, L. Martin-Samos, N. Marzari, F. Mauri, R. Mazzarello, S. Paolini, A. Pasquarello, L. Paulatto, C. Sbraccia, S. Scandolo, G. Sclauzero, A. P. Seitsonen, A. Smogunov, P. Umari, R. M. Wentzcovitch, J. Phys.: Condens. Matter 2009, **21**, 395502.

[25] J.P. Perdew, K. Burke, M. Ernzerhof, Physical Review Letters 1996, **77**, 3865.

[26] V. Barone, M. Casarin, D. Forrer, M. Pavone, M. Sambi, A. Vittadini, J. Comput. Chem. 2009, **30**, 934.

[29] H. J. Monkhorst, J. D. Pack, Phys. Rev. B 1976, **13**, 5188.

[30] D.W. Boukhvalov, E.Z. Kurmaev, A. Moewes, D. A. Zatsepin, V.M. Cherkashenko, S. N. Nemnonov, L.D. Finkelstein, Y.M. Yarmoshenko, M. Neumann, V.V. Dobrovitski, M.I. Katsnelson, A.I. Lichtenstein, B.N. Harmon, P. Kögerler, Phys. Rev. B 2003, **67**, 134408.

[31] P.W. Anderson, Solid State Phys. 1963, **14**, 99.

[32] B. Heinrich, J. Cochran, Adv. Phys. 1993, 42, 523.

[33] A. A. Katanin, V. Y. Irkhin, Physics-Uspekhi 2007, 50, 613.

[34] H. v. Löhneysen, A. Rosch, M. Vojta, P. Wölfle, Rev. Mod. Phys. 2007, **79**, 1015.

[35] J. Červenka, M. Katsnelson, C. Flipse, Nat. Phys. 2009, **5**, 840.

[36] T.L. Makarova, A.L. Shelankov, I. Serenkov, V. Sakharov, D. Boukhvalov, Phys. Rev. B 2011, **83**, 085417.

[37] M. Sepioni, R.R. Nair, I.-L. Tsai, A.K. Geim, I.V. Grigorieva, Europhys. Lett. 2012, **97**, 47001.

Nanoscale Accepted Manuscript